Author's Accepted Manuscript

Confinement of Carbon Dots Localizing to the Ultrathin Layered Double Hydroxides Toward Simultaneous Triple-mode Bioimaging and Photothermal Therapy

Yangziwan Weng, Shanyue Guan, Heng Lu, Xiangmin Meng, Abdessamad. Y Kaassis, Xiaoxue Ren, Xiaozhong Qu, Chenghua Sun, Zheng Xie, Shuyun Zhou

Cite this article as: Yangziwan Weng, Shanyue Guan, Heng Lu, Xiangmin Meng, Abdessamad. Y Kaassis, Xiaoxue Ren, Xiaozhong Qu, Chenghua Sun, Zheng Xie and Shuyun Zhou, Confinement of Carbon Dots Localizing to the Ultrathin Layered Double Hydroxides Toward Simultaneous Triple-mode Bioimaging and Photothermal Therapy, *Talanta,* https://doi.org/10.1016/j.talanta.2018.02.093

Confinement of Carbon Dots Localizing to the Ultrathin Layered Double Hydroxides Toward Simultaneous Triple-mode Bioimaging and Photothermal Therapy

Yangziwan Weng[a], Shanyue Guan[a*], Heng Lu[a], Xiangmin Meng[a], Abdessamad. Y Kaassis[b], Xiaoxue Ren[a], Xiaozhong Qu[c], Chenghua Sun[*a], Zheng Xie[a], Shuyun Zhou[*a1]

[a] Key Laboratory of Photochemical Conversion and Optoelectronic Materials, Technical Institute of Physics and Chemistry, Chinese Academy of Sciences, Beijing, 100190, China.

[b] School of Chemistry and Pharmacy, University of East Anglia, Norwich Research Park, Norwich, Norfolk, NR4 7TJ, UK

[c] College of Materials Science and Opto-Electronic Technology, University of Chinese Academy of Sciences, Beijing 100190, China.

guanshanyue@mail.ipc.ac.cn;
sunchenghua@mail.ipc.ac.cn;
zhou_shuyun@mail.ipc.ac.cn

ABSTRACT

It is a great challenge to develop multifunctional nanocarriers for cancer diagnosis and therapy. Herein, versatile CDs/ICG-uLDHs nanovehicles for triple-modal fluorescence/photoacoustic/two-photon bioimaging and effective photothermal therapy were prepared *via* a facile self-assembly of red emission carbon dots (CDs), indocyanine green (ICG) with the ultrathin layered double hydroxides (uLDHs). Due to the J-aggregates of ICG constructed in the self-assembly process, CDs/ICG-uLDHs was able to stabilize the photothermal agent ICG and enhanced its photothermal efficiency. Furthermore, the unique confinement effect of uLDHs has extended the fluorescence lifetime of CDs in favor of bioimaging. Considering the excellent *in vitro* and *in vivo* phototherapeutics and multimodal imaging effects, this work provides a promising platform for the construction of multifunctional theranostic nanocarrier system for the cancer treatment.

Keywords:
Carbon dots; Ultrathin layered double hydroxides; Triple-mode imaging Photothermal therapy

1. Introduction

Theranostics, combining therapeutic modalities and diagnostic imaging is a promising cancer therapy for concurrent monitoring and individualized treatment [1-2]. Generally, an appropriate imaging technique is a crucial part of theranostics system to precisely observe the growth and location of tumors for efficient cancer therapy and specific diagnosis. The common diagnosis approaches contain fluorescence (FL) imaging, magnetic resonance imaging (MRI), computed tomography (CT), photoacoustic (PA) imaging and so on [3-5]. Among those techniques, FL imaging is one of the most effective techniques due to its non-invasiveness, high sensitivity and simplicity for realization [6]. However, the spatial resolution of the PL imaging is not satisfaction due to its limited penetration depth [7]. On the contrary, two-photon fluorescence imaging has attracted attention owing to its higher spatial resolution induced by longer excitation wavelength [8]. In addition, PA imaging utilizes short laser pulses to generate the ultrasonic waves and provides deeper biological tissue imaging as a state-of-the-art technique [9-10]. Therefore, integrating FL and PA with two-photon fluorescence imaging into one technique can be beneficial for the cancer diagnosis, especially for detection of deeper tissues with excellent sensitivity and resolution.

1
  Fax: +86 10 62554670 Tel: +86 10 82543428

Carbon dots (CDs) have emerged as a new class of efficient fluorescence imaging agents for its attractive properties, such as high water dispersity, excellent biocompatibility, low toxicity [11-13]. A large variety of fluorescence tags based on carbon dots have been investigated. However, most of the reported CDs are blue or green light emission [14-15], which limits its deep penetration application in biomedicine [7, 16]. Additionally, most CDs possess up-conversion photoluminescence (UCPL) [17-19], but only a few studies have reported this property in bioimaging. Therefore, the development of an effective method to prepare red-emission CDs with higher quantum yield for both FL and two-photon fluorescence imaging for cancer theranostics may offer a new opportunity for CDs in the biomedical field.

Another essential part for the theranostics is cancer therapy. The traditional cancer therapy such as radiotherapy, chemotherapy often suffer from severe side effects [20]. This motivates us to find an alternative way with minimal side effects. Photothermal therapy as an emerging therapeutic modality, has received much attention for its controllable, non-invasive property [21-22]. This light-triggered therapy relies on the photothermal agents to convert light energy to heat and induces tumor cells apoptosis [23]. A variety of photothermal agents (e.g., copper sulfide, golden nanorod, small organic molecules) [1, 24-25] have been developed. However, they suffer from a few problems, for instance poor water dispersion, high toxicity and metabolizability [26]. To overcome those drawbacks, the photothermal agents can be encapsulated within, or attached to, a carrier, such as polymeric carriers, inorganic nanoparticles, liposome, metal organic framework and so on [27-29]. Among them, the two-dimensional (2D) layered material has attracted tremendous attention for its unique structure and properties [30-31], such as high specific surface area, ultrathin thickness, unique electron structure, anisotropic physical and chemical properties [32]. Meanwhile, it is convenient for the modification of the two-dimensional (2D) material with multiple functionalities such as targeting and bioactivity with high drug loading capacity [33-35]. These endow 2D nanomaterials great potentials for a wide range of applications in the biomedical field.

Layered double hydroxides (LDHs), one of the emerging 2D inorganic layered materials, have intrigued researchers interest in the biomedical area [36-39]. Utilizing the adaptability of its chemical composition [20], controllable particle size and the anionic exchange properties [40-41], LDHs have been widely applied towards the cancer research [26, 41]. Although the intercalated-LDHs materials possess good therapeutic effect, some of them suffer from poor water dispersity, low loading capacity. To improve those disadvantages, the LDHs can be exfoliated into unilamellar form, a new type of nanosheets with two-dimensional (2D) anisotropy and positive charge [42-43]. It can be served as an ideal building block or substrate, exhibiting unconventional physicochemical properties, such as surface confinement effect, higher loading capacity, good water dispersity and stability [44-45]. This can be motivating area, where ultrathin LDHs can be employed as a novel platform to achieve multifunctional cancer theranostics.

Herein, we adopt one-step synthesis of the ultrathin layered double hydroxides (uLDHs) to develop a multifunctional nanovehicle (denoted as CDs/ICG-uLDHs). As depicted in Scheme 1, the red emission carbon dots and indocyanine green (ICG, a photothermal agent) [46-47] were incorporated to uLDHs *via* self-assembly. As expected, this CDs/ICG-uLDHs agent expresses excellent fluorescence features detected by confocal microscopy imaging, two-photon imaging and fluorescence lifetime imaging [48-49]. Considering the efficient absorbance in the NIR region, CDs/ICG-uLDHs is also capable of photoacoustic imaging. In this study, the outstanding therapeutic effect and imaging properties of CDs/ICG-uLDHs can be found in both *in vivo* and *in vitro* studies. Hence, this CDs/ICG-uLDHs material exhibits great potential for efficient cancer imaging and therapy.

2. Results and Discussion

2.1 Structural and Morphological Characterization

2
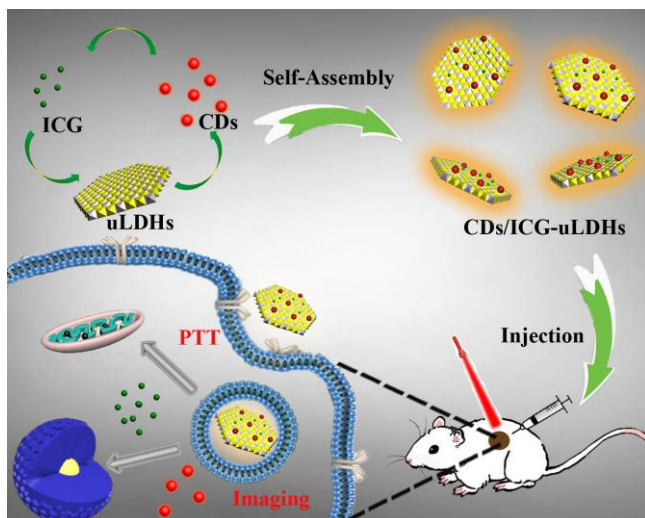
Schematic 1 Schematic illustration of CDs/ICG-uLDHs nanocomposite as a nanovehicle for imaging and therapy.

The uLDHs were prepared *via* the one-pot method [50] and its structural characterizations were carried out by X-ray diffraction (XRD) in Figure 1a. The XRD of CDs-ICG/uLDHs exhibits typical (00l) characteristic peaks with the corresponding (003) reflection at 11.47° in accord with uLDHs. The diffraction peak is caused by the re-stacked colloidal uLDHs nanosheets, while this dispersion sample was dried onto a glass to prepare the XRD sample. Additionally, both virtually transparent uLDHs solution and red CDs/ICG-uLDHs solution exhibit obvious a Tyndall effect, indicating the existence of colloidal uLDHs in solution (Figure 1a, inset). The samples were further investigated by Fourier transform infrared spectra (FT-IR) (Figure 1b) to characterize the chemical bonds and functional groups of CDs/ICG-uLDHs. The typical IR bands of CDs at 3406 cm^{-1}, 3182 cm^{-1}, 1234 cm^{-1}, 1647 cm^{-1} can be attributed to the O–H, N–H, C–O, –COOH, respectively. These bands can enhance the water dispersity of CDs. Additionally, the stretching vibrations of C–H (2924 cm^{-1}, 2854 cm^{-1}), C=C (1516 cm^{-1}), C–N= (1323 cm^{-1}) indicate that the CDs are formed of polyaromatic [19]. The FT-IR spectrum of CDs/ICG-uLDHs is almost similar with the CDs. However, the absorption band at 890 cm^{-1} of CDs/ICG-uLDHs can be assigned to the out-of-plane bending vibration of isolated hydrogen in the benzene ring of ICG [51]. The characteristic band of uLDHs at 1381 cm^{-1} in Figure S1 is assigned to the vibration mode of CO_3^{2-}, indicating the carbonate LDHs [52-53]. In addition, the X-ray photoelectron spectroscopy (XPS) surveys (Figure S2) of CDs, uLDHs and CDs/ICG-uLDHs can further confirm the FT-IR data. The full spectrum of CDs demonstrates that the CDs exhibits the signals of C, N, O elements. Compared with uLDHs, the similar peaks of Mg and Al in the CDs/ICG-uLDHs indicate the existence of uLDHs. The introduction of slight S in CDs/ICG-uLDHs is caused by the adsorption of ICG. In detail, the high-resolution XPS spectra of CDs/ICG-uLDHs show that the C 1s peak can be deconvoluted into four peaks, namely, C–C/C=C (284.6 eV), C–N (285.3 eV), C–O (286.2 eV) and –COOH (288.8 eV) (Figure S2b) [54], which is consistent with the FT-IR results.
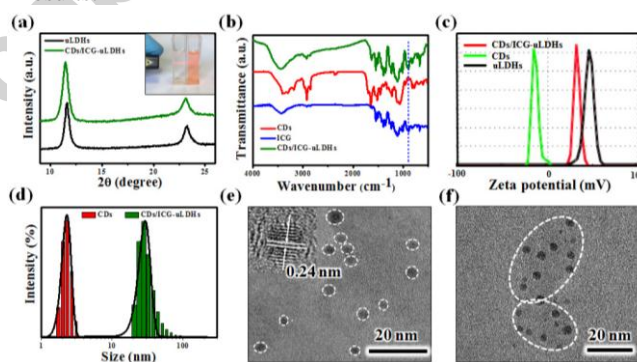
Fig. 1. (a) XRD patterns of uLDHs and CDs/ICG-uLDHs. The inset exhibits the Tyndall effect of uLDHs and CDs/ICG-uLDHs. (b) FT-IR spectra of CDs, ICG and CDs/ICG-uLDHs, respectively. (c) Zeta potential of CDs, uLDHs and CDs/ICG-uLDHs, respectively. (d) Size distribution of CDs and CDs/ICG-uLDHs was investigated by DLS measurements. HRTEM images of (e) CDs and (f) CDs/ICG-uLDHs, respectively, and the inset in (e) displays the lattice fringe of CDs.

Furthermore, the Zeta potential of CDs, ICG and uLDHs was investigated in the aqueous solution (Figure 1c). The obtained CDs are negatively-charged with a Zeta potential of −11.7 mV for the existence of carboxyl groups on the surface, while uLDHs are positive-charged with a Zeta potential of +48 mV. Due to the interaction among CDs, ICG and uLDHs (electrostatic force

and hydrogen bonding), the CDs/ICG-uLDHs displays a high Zeta potential of +31.9 mV, indicating its good stability in the aqueous solution. The stability of this agent in the physiologic solution of phosphate buffered solution (PBS) was further investigated through UV-vis spectra. As shown in Figure S3, the absorption of ICG has declined by 85 % rapidly within 10 days, while the curve of CDs/ICG-uLDHs shows a slow decline of 20 %. The fact reveals that the nanoparticles have maintained excellent stability in an aqueous solution. Additionally, the hydrodynamic diameter of CDs was measured to be 2–5 nm by dynamic light scattering (DLS) (Figure 1d, red column). After integrating with uLDHs and ICG, the size of CDs/ICG-uLDHs agent has grown, ranging from 20–50 nm (Figure 1d, green column), which is similar to the uLDHs (Figure S4). The morphology of uLDHs nanosheets was explored using the atomic force microscopy (AFM) and the data are shown in Figure S5. The data exhibit that the lateral width of uLDHs was less than 0.50 nm, suggesting the presence of the ultrathin nanosheet [31]. Next, the high-resolution transmission electron microscopy (HRTEM) was carried out, and the uLDHs show a uniform plate-like structure with a lattice fringe of 0.197 nm that can be assigned to the (110) plane of LDH (Figure S6) [40]. Furthermore, the TEM images of CDs and CDs/ICG-uLDHs are depicted in Figure 1e-f. As indicated in Figure 1e, CDs demonstrated the uniformed morphology with the particle size around 2.30 nm (Figure S7), which is close to the DLS results. The inset in Figure 1e displays crystal lattice of 0.24 nm, which is consistent with the (100) in-plane lattice of graphene [54]. The uniformly dispersed CDs in uLDHs nanosheets can be found in HRTEM (Figure 1f and Figure S8), revealing the successful self-assembly of CDs on the uLDHs.
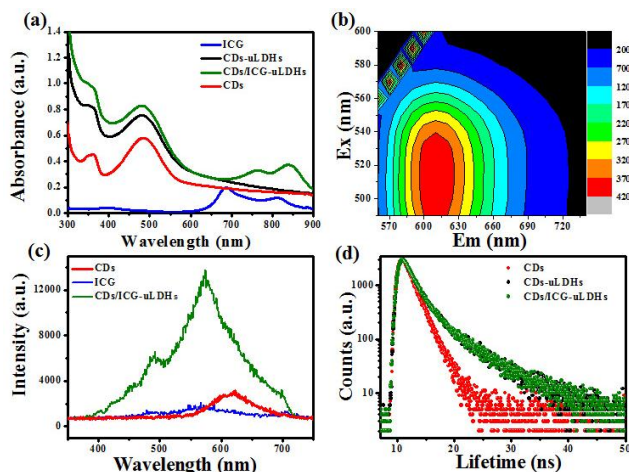

Fig. 2. (a) UV-vis absorption spectra of CDs, ICG, CDs-uLDHs and CDs/ICG-uLDHs, respectively. (b) 3D fluorescence spectrum of CDs. (c) UCPL spectra (800 nm femtosecond pulsed laser was throughout applied) of CDs, ICG, and CDs/ICG-uLDHs, respectively. (d) Fluorescence lifetime of CDs, CDs-uLDHs and CDs/ICG-uLDHs.

Next, we explore the ultraviolet-visible (UV-vis) absorption spectra of CDs, CDs-uLDHs and CDs/ICG-uLDHs, uLDHs, ICG, ICG-uLDHs, respectively. The pristine CDs reveal an obvious absorption peak centered at 495 nm (Figure 2a). Furthermore, two absorption peaks at 687 and 808 nm can be detected for the ICG in aqueous solution. When ICG, CDs were loaded to the uLDHs, the absorption peaks of ICG are red shifted to 767 and 841 nm, respectively (Figure 2a and S9). The red-shift at 841 nm is due to the J-aggregates of ICG caused by uLDHs. It is a type of supramolecular self-organization, meaning the dye is aggregated by the "vicinity effect" of the adjacent molecules accompanied by changes in the absorption spectrum [55]. Herein, the uLDHs structure and the interaction such as electrostatic force and hydrogen bonding between ICG and uLDHs, aided ICG into self-assembly arrangement on the surface of uLDHs, resulting in a coherent conjugated system and π-electrons delocalizing over the large extended [56]. As a consequence, J-aggregate state can be obtained, which is in favor of theranostics application for ICG.

To explore the photoluminescence property of CDs, CDs-uLDHs and CDs/ICG-uLDHs, Figure S10a presents the PL spectra of these samples. CDs, CDs-uLDHs and CDs/ICG-uLDHs exhibit similar emission performance with emission peaking at 620 nm under 495 nm irradiation. Additionally, the corresponding 3D fluorescence spectra was measured (Figure 2b), and the data reveal the luminescence center of CDs is mainly located in the red area. Furthermore, it is found that the CDs has two-photon fluorescence emission at 620 nm under 800 nm irradiation, which is similar to CDs-uLDHs (Figure S10b). The relationship between laser powers and integration area of PL intensities matches quadratic dependence, which demonstrates that the up-conversion photoluminescence (UCPL) emission of CDs is a two-photon excitation process (Figure S10c-d) [19]. As shown in Figure 2c, CDs/ICG-uLDHs acutely exhibits higher UCPL intensity than free CDs and ICG. Furthermore, UCPL properties of ICG-uLDHs and CDs/ICG-uLDHs were almost similar shown in Figure S11, which indicates the J-aggregates of ICG was induced by the confinement of the uLDHs and resulted in better UCPL property of CDs/ICG-uLDHs, while uLDHs failed to emit under 800 nm laser irradiation. This outstanding two-photon fluorescence property of the agent could have the potentials towards bioimaging field.

4

In this work, this red emitting CDs were prepared by our group [57]. Compared with traditional green or blue CDs, the red CDs displays fewer light absorption and can enhance penetration depth of living tissues [58]. The quantum yield (QY) of this CDs is up to 32.9 % under the 495 nm irradiation, which is better than the majority reported red emitting CDs [54, 59-60]. This is beneficial for the cancer imaging. The corresponding parameters are shown in Figure S12. The fluorescent lifetime is another essential property for the optical functional materials. Thus, we examined the lifetime of the CDs, CDs-uLDHs and CDs/ICG-uLDHs under the excitation of 485 nm. The average fluorescence lifetime of CDs-uLDHs (2.98 ns) is twice longer than that of pristine CDs solution (1.58 ns) (Figure 2d and Table S1), while the lifetime of CDs/ICG-uLDHs (3.08 ns) is similar with CDs-uLDHs. According to the previous reports [14, 61], the unique two-dimensional confinement effect of LDHs shows fascinating effects, for instance speeding up the chemical reactions [61] and prolonging the lifetime of Au nanocluster [44]. These enlighten our reflections upon the confinement effect of uLDHs for extension of the lifetime of CDs. Based on the band gap theory, if the excited electrons are effectively confined by the substrate such as uLDHs, it provides an effective way to extend fluorescence lifetime. In order to prove whether the excited electrons can be restricted by uLDHs, the Nyquist plot of the electrochemical impedance spectroscopy (EIS) was introduced to research the electron mobility of CDs and CDs/ICG-uLDHs [44, 62]. As shown in Figure S13, the electron mobility of CDs is larger than that of CDs/ICG-uLDHs, which proves uLDHs possess great electron confinement effect so as to delay electron hole recombination time and thus promoting fluorescence lifetime.
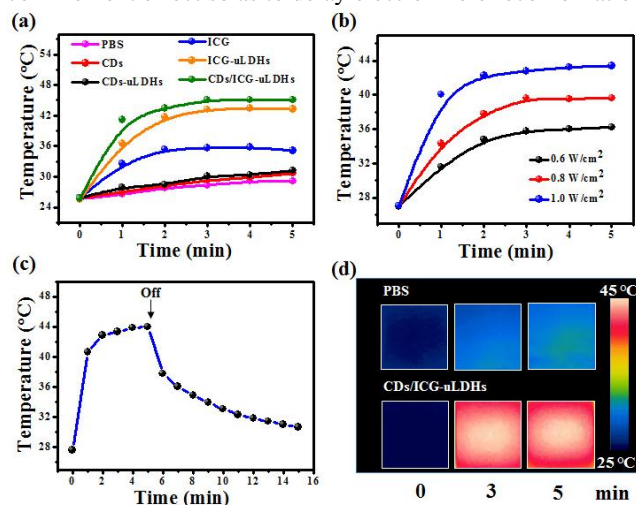
Fig. 3. (a) Temperature elevation of various aqueous solutions under irradiation with an 808 nm NIR laser at a power of 1.0 W/cm^2. (b) Temperature elevation of CDs/ICG-uLDHs aqueous solution under different power densities. (c) The monitored temperature profile CDs/ICG-uLDHs aqueous solution under irradiation with an 808 nm laser for 5 mins, followed by the laser turned off. (d) Thermal images of PBS and CDs/ICG-uLDHs under 808 nm laser (1.0 W/cm^2) irradiation for 5 min. The CDs, CDs/uLDHs, CDs/ICG-uLDHs solution contained same quantity of CDs (50 ug/mL).

Another essential property of CDs/ICG-uLDHs is the tunable photothermal effects. In order to evaluate this photothermal effect, the temperature elevation of PBS, CDs, CDs-uLDHs, ICG, ICG-uLDHs and CDs/ICG-uLDHs aqueous solutions were recorded under irradiation of an 808 nm NIR laser at a power of 1.0 W/cm^2. As it is indicated in Figure 3a, upon the 808 nm NIR laser, CDs and CDs-uLDHs aqueous solution didn't induce obvious temperature increase, which is similar with PBS. By contrast, as a typical photothermal agent, the presence of pristine ICG aqueous solution did promote this photothermal process, and the temperature was elevated to 36 ℃ within 300 s. When it was incorporated with uLDHs, the temperature of ICG-uLDHs aqueous solution was further elevated to 43 ℃ at same concentration of ICG, indicating the uLDHs can contribute to light heat conversion efficiency of ICG solution. In particular, the CDs/ICG-uLDHs sample reveals the best photothermal conversion performance, where the temperature was enhanced from 25 ℃ to 45 ℃ after the NIR irradiation for 300 s. Then, the CDs/ICG-uLDHs solutions were further exposed to the 808 nm laser at various power densities from 0.6 to 1.0 W/cm^2 for 5 min (Figure 3b). The results demonstrate that the temperature goes up as the laser power density increases. To further investigate the photothermal conversion efficiency of CDs/ICG-uLDHs, the temperature change of the solution was recorded as a function of time, when the laser was shut off after 5 min irradiation (Figure 3c). The temperature gradually decreased without NIR irradiation, confirming that the NIR laser is the essential resource for the temperature enhancement of aqueous CDs/ICG-uLDHs solution. Additionally, the thermal behavior of CDs/ICG-uLDHs was monitored by an infrared thermal imaging camera (Figure 3d). Compared with PBS solution, the CDs/ICG-uLDHs shows brighter red thermal image, visually indicating the excellent photothermal effect of CDs/ICG-uLDHs agent for anticancer therapy.

2.2 *In vitro* study of CDs/ICG-uLDHs.
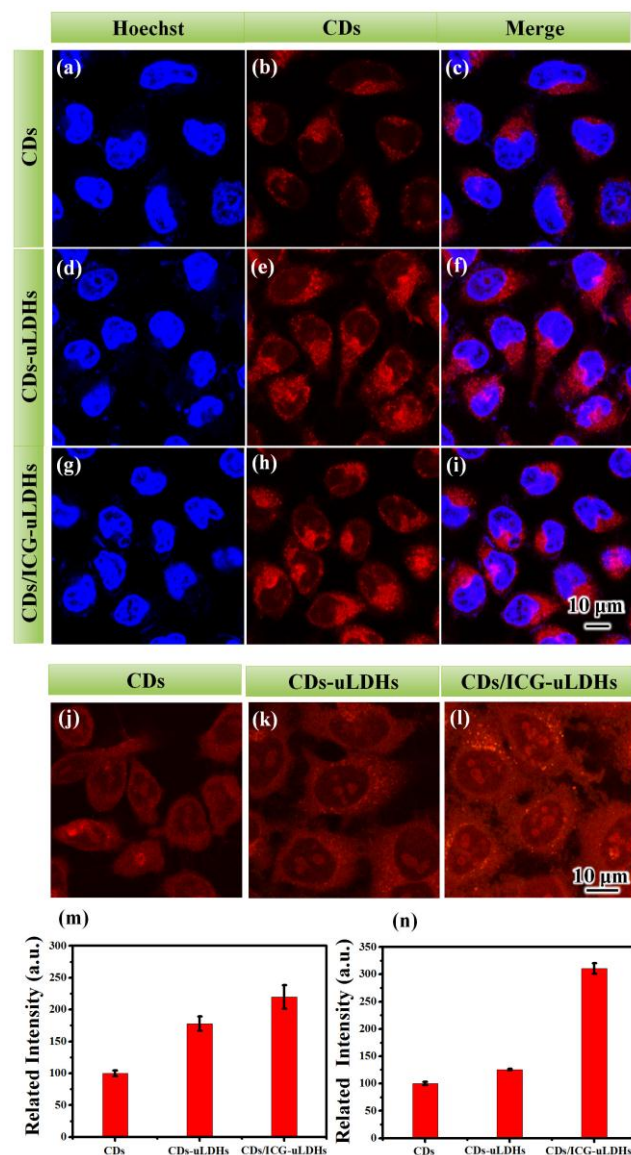
Fig.4. Confocal laser scanning microscopy images of Hela cells incubated with CDs (a-c), CDs-uLDHs (d-f) and CDs/ICG-uLDHs (g–i) for 24 h under the excitation of 488 nm. Two-photon fluorescence imaging of CDs (j), CDs-uLDHs (k) and CDs/ICG-uLDHs (l) under the excitation of 808 nm. Confocal fluorescence intensity (m) and two-photon fluorescence intensity (n) of CDs, CDs-uLDHs and CDs/ICG-uLDHs. The CDs, CDs/uLDHs, CDs/ICG-uLDHs solution contained same quantity of CDs (50 ug/mL).

The excellent optical property and photothermal effect of CDs/ICG-uLDHs make it an appropriate agent toward cancer imaging. We first probed the confocal imaging by the Hela cells. As indicated in Figure 4, the Hela cells were incubated with the CDs, CDs-uLDHs and CDs/ICG-uLDHs, respectively, while the cells' nucleus were stained with Hoechst and indicate blue color. For the pristine CDs sample, the cells revealed an obvious red color (Figure 4b), indicating that the effective uptake by the Hela cells. After incorporation with uLDHs, the cells manifest stronger red fluorescence intensity than the pristine CDs (Figure 4d-f and 4m). This is caused by an increase in the uptake of uLDHs. Furthermore, compared with the CDs and CDs-uLDHs, the CDs/ICG-uLDHs sample exhibited the strongest fluorescence intensity due to the intrinsic red fluorescence of CDs and ICG (Figure 4g-4i). The average pixels of imaging zones were calculated, and the fluorescence intensity of CDs/ICG-uLDHs was 2.2-folds stronger than that of CDs. Besides, the similar confocal imaging ability can also be found in the HepG-2 cells (Figure S14).

Owing to the intrinsic two-photon fluorescence property of CDs, we further probed the two-photon fluorescence imaging of Hela cells incubated with CDs, CDs-uLDHs and CDs/ICG-uLDHs, respectively. The strong two-photon fluorescence emission from cells can be observed in Figure 4j-4l. The intensity increased as follows: CDs < CDs-uLDHs < CDs/ICG-uLDHs, which is similar with the confocal imaging (Figure 4n). Owing to the various fluorescence lifetime of these three samples, fluorescence lifetime imaging microscopy (FLIM) is considered *in vitro* (Figure S15). In accordance with the experimental results in solution,

6

the CDs-uLDHs and CDs/ICG-uLDHs have longer lifetime than CDs *in vitro* (Table S2), because the excited electrons of CDs can be efficient restricted by the uLDHs and lead to longer lifetime of CDs-uLDHs and CDs/ICG-uLDHs.
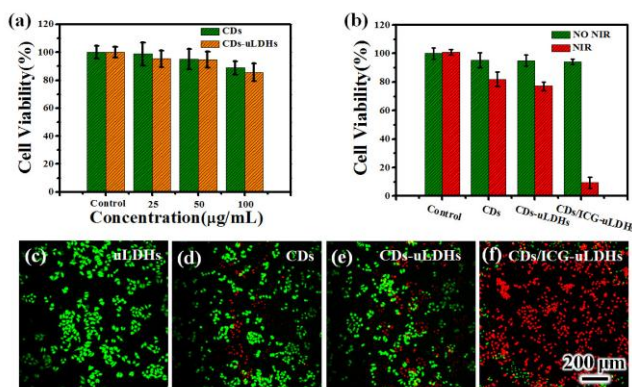
Fig.5. (a) *In vitro* viability tests of Hela cells treated with CDs and CDs-uLDHs for 24 h. (b) Viability of Hela cells treated with CDs, CDs-uLDHs and CDs/ICG-uLDHs, respectively under dark and 808 nm irradiation with the intensity power of 1.0 W/cm^2 for 5 min. Confocal imaging of uLDHs (c), CDs (d), CDs-uLDHs (e) and CDs/ICG-uLDHs (f) under the NIR irradiation. Live Hela cells present green and dead are red (Calcein AM/PI). The CDs, CDs/uLDHs, CDs/ICG-uLDHs solution contained same quantity of CDs (50 ug/mL) in Figure b, d, e, f, while the contents of uLDHs and ICG were 200 µg/mL and 8 µg/mL.

To evaluate the photothermal properties of CDs, CDs-uLDHs and CDs/ICG-uLDHs samples against the Hela cells, the Hela cells were incubated with these three samples for 24 h and then exposed to 808 nm laser at 1 W/cm^2 for 5 min. As displayed in Figure 5a, the viabilities of CDs and CDs-uLDHs remain 90 % and 86 %, respectively, at the maximum concentration of CDs (100 µg/mL). This reveals the biocompatibility of CDs and CDs-uLDHs. In addition, there is no significant cytotoxicity of CDs, CDs-uLDHs and CDs/ICG-uLDHs without NIR irradiation (Figure 5b). After the NIR irradiation, the viabilities of CDs, CDs-uLDHs slightly decrease to 82 % and 78 %. By contrast, the viability of CDs/ICG-uLDHs plummets to 8.9 %, demonstrating a remarkable cells damage under the NIR irradiation. The enhanced cellular uptake and the efficient conversion from light to heat of CDs/ICG-uLDHs are the main reasons for the cells damage. To visualize the PTT effect of the samples, the live cells were stained by Calcein AM with green fluorescence and dead cells were stained by propidium iodide (PI) with red fluorescence. Their confocal imaging was recorded and depicted in Figure 5f. The confocal microscopy images show that Hela cells treated with the uLDH sample (Figure. 5c) display no obvious death, and the CDs, CDs-uLDHs showed ineffective treatment under the NIR irradiation as well. However, the CDs/ICG-uLDHs generated the strongest red fluorescence singal, which demonstrates that CDs/ICG-uLDHs has the best anticancer effectiveness under the NIR irradiation.

2.3 *In vivo* study of CDs/ICG-uLDHs.
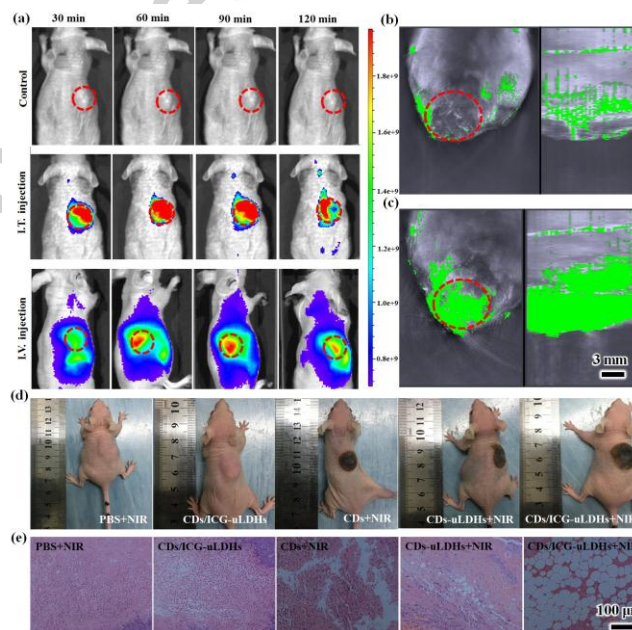
Fig.6. (a) Real-time *in vivo* fluorescence images obtained after intratumoral and intravenous injections of CDs/ICG-uLDHs in nude mice at different time points. The 3D multi-spectral optoacoustic tomography (MSOT) image and enlarged orthogonal views of tumor before (b) after (c) the injection of CDs/ICG-uLDHs under 808 nm laser irradiation (d)

7

Representative photographs of tumor-bearing mice at 15 days and (e) the H&E-stained tumor sections after treatment with PBS+NIR, CDs/ICG-uLDHs, CDs+NIR, CDs-uLDHs+NIR and CDs/ICG-uLDHs+NIR, respectively (808 nm, 1.0 W/cm^2, 10 min).

To further evaluate the ability of CDs/ICG-uLDHs agent as a useful *in vivo* theranostics platform, we explore its feasibility for *in vivo* imaging guided PTT. Initially, 100 μL CDs/ICG-uLDHs was injected intra-tumor into the Hela tumor-bearing male nude Balb/c mice, while 100 μL PBS was selected as the control group. As depicted in Figure 6a, the CDs/ICG-uLDHs sample had gradually accumulated in the tumor area after 30 min under the excitation of 495 nm compared with control group. Then, the mice were sacrificed. The organs (e.g. heart, lung, liver, spleen, kidneys and tumors) were excised and their fluorescence images were recorded (Figure S16). The excised tumor tissue showed stronger florescence signal, while the rest of organs revealed rather low signals. This can demonstrate that the CDs/ICG-uLDHs is mainly accumualted in the tumor site. To further investigate the FL imaging *in vivo*, the tumor bearing mice were treated with 100 μL CDs/ICG-uLDHs *via* tail vein injection. The FL signals were collected at different time points (Figure 6a), which indicates the agent can favourably accumulate in the tumor. Considering the efficient absorbance in the NIR region, we further probed the feasibility of CDs/ICG-uLDHs for in vivo photoacoustic imaging (PAI). As indicated in Figure 6b, there is no PAI singal that can be detected in the turmor site before the injection of CDs/ICG-uLDHs. This implies that the tumor itself cannot trigger the PAI singal. After the tumor site injection of CDs/ICG-uLDHs, the strong green PAI singal can be detected at the 808 nm irradiation in Figure 6c. The corrsponding mean intensity of the region of interest (ROI) exhibits significant enhancement PAI intensity after the injection of CDs/ICG-uLDHs (Figure S17). This shows that the CDs/ICG-uLDHs can be a potential PAI contrast agent for *in vivo* imaging.

In order to evaluate the therapeutic performance of the CDs/ICG-uLDHs agent *in vivo*, five groups of Hela tumor-bearing nude mice with five mice per group were used in our experiment, including CDs+NIR, CDs-uLDHs+NIR, CDs/ICG-uLDHs+NIR, PBS+NIR and CDs/ICG-uLDHs without NIR. The solutions of the CDs, CDs-uLDHs, CDs/ICG-uLDHs were dosed intratumorally at a level of 8 mg/kg and 2.4 mg/kg for CDs and ICG, respectively, while100 μL PBS was injected to the control group. Then the tumors were exposed to an 808 nm laser at 1.0 W/cm^2 for 10 min, except the CDs/ICG-uLDHs control group. As shown in Figure S18, the growth of the tumor was totally prevented in the light-mediated CDs/ICG-uLDHs group, compared with the other groups. In addition, the tumor-bearing mice treated with CDs and CDs-uLDHs under the 808 nm irradiation also demonstrate a moderate tumor inhibition performance. As we know, CDs are a carbon-based material and can generate hyperthermia under the NIR irradiation [7, 22, 63]. The concentration of CDs in the *in vitro* experiment is 50 μg/mL, while the concentration *in vivo* of CDs is 2 mg/mL. The increased concentration of CDs can enhance the temperature elevation (Figure S19). This can explain the tumor suppression by the CDs and CDs-uLDHs. In contrast, tumors in the CDs/ICG-uLDHs without NIR group continued to grow rapidly, indicating the nontoxicity of CDs/ICG-uLDHs agent without NIR. It is worth noting that the tumor treated with CDs/ICG-uLDHs+NIR displayed an apparent effect on suppressing the tumor growth, which verifies its high efficacy light-mediated PTT anticancer performance. The representative photographs of tumor-bearing mice from different groups were taken at 15 days after treatments. As shown in Figure 6d, the tumor sites from CDs+NIR, CDs-uLDHs+NIR, CDs/ICG-uLDHs+NIR all showed a black scar after PTT treatment, showing effective treatment effect. More intuitively, the mice were sacrificed and the excised tumors from representative Balb/c mice after 15 days treatment were presented in Figure S20. Furthermore, the excised tumors were analyzed by hematoxylin and eosin (H&E)-stained to investigate the PTT effect and potential toxicity of samples. A large area of the tumor tissues were necrotic for the CDs/ICG-uLDHs+NIR, whereas a fraction of necrosis tumor cells occurred in CDs+NIR and CDs-uLDHs+NIR (Figure 6e). However, no obvious cell apoptosis can be observed in PBS control group and CDs/ICG-uLDHs without NIR. In addition, the H&E images of major organs treated with CDs/ICG-uLDHs+NIR showed negligible organ damage induced by light-mediated CDs/ICG-uLDHs (Figure S21). All results confirm that CDs/ICG-uLDHs can act as an ideal theranostic agent for efficient cancer imaging and therapy.

3. Conclusions

In summary, we have fabricated a novel multifunctional cancer theranostics platform *via* the incorporation of CDs and ICG with the ultrathin layered double hydroxides, which combined triple-mode imaging and efficient PTT treatment. *In vitro* tests revealed that the CDs/ICG-uLDHs agent exhibited an excellent imaging and efficient phototherapy performance, while *in vivo* studies further confirm the outstanding fluorescent imaging, photoacoustic imaging performance and tumor inhibition ability of CDs/ICG-uLDHs under the 808 nm irradiation. Hence, this work provides a simple and effective method in the design and fabrication of 2D ultrathin material with significantly enhanced biocompatibility, fluorescent imaging properties and outstanding anticancer activity, which can be potentially applied in biomedical fields.

References

[1] Y. Yang, C. Yue, Y. Han, W. Zhang, A. He, C. Zhang, T. Yin, Q. Zhang, J. Zhang, Y. Yang, Adv. Funct. Mater. 26 (2016) 8735–8745.
[2] L. Han, Y. Zhang, Y. Zhang, Y. Shu, X.W. Chen, J.H. Wang, Talanta 171 (2017) 32–38.
[3] L. Wang, H. Xing, S. Zhang, Q. Ren, L. Pan, K. Zhang, W. Bu, X. Zheng, L. Zhou, W. Peng, Y. Hua, J. Shi, Biomaterials 34 (2013) 3390–3401.
[4] B. Shi, X. Gu, Q. Fei, C. Zhao, Chem. Sci. 8 (2017) 2150–2155.
[5] J. Peng, M. Dong, B. Ran, W. Li, Y. Hao, Q. Yang, L. Tan, K. Shi, Z. Qian, ACS Appl. Mater. Interfaces 9 (2017) 13875–13886.
[6] X. Liang, L. Fang, X. Li, X. Zhang, F. Wang, Biomaterials 132 (2017) 72–84.
[7] J. Ge, Q. Jia, W. Liu, Adv. Mater. 27 (2015) 4169-4177.
[8] P. Ning, P. Dong, Q. Geng, L. Bai, Y. Ding, X. Tian, R. Shao, L. Li, X. Meng, J. Mater. Chem. B 5 (2017) 2743–2749.
[9] Y. Liu, S. Wang, Y. Ma, J. Lin, H.Y. Wang, Y. Gu, X. Chen, P. Huang, Adv. Mater. 29 (2017) 1606129–1606134.
[10] X. Zhen, X. Feng, C. Xie, Y. Zheng, K. Pu, Biomaterials 127 (2017) 97–106.
[11] X.T. Zheng, A. Ananthanarayanan, K.Q. Luo, P. Chen, Small 11 (2015) 1620–1636.
[12] M. Han, L. Wang, S. Li, L. Bai, Y. Zhou, Y. Sun, H. Huang, H. Li, Y. Liu, Z. Kang, Talanta 174 (2017) 265–273
[13] S. Hu, Y. Zhou, C. Xue, J. Yang, Q. Chang, Chem. Commun. 53 (2017) 9426–9429.
[14] N. Xue, X. Kong, B. Song, L. Bai, Y. Zhao, C. Lu, W. Shi, Solar RRL. 1 (2017) 1700029–1700036.
[15] M.J. Meziani, X. Dong, L. Zhu, L.P. Jones, G.E. LeCroy, F. Yang, S. Wang, P. Wang, Y. Zhao, L. Yang, R.A. Tripp, Y.P. Sun, ACS Appl. Mater. Interfaces 8 (2016) 10761–10766.
[16] X. Miao, X. Yan, D. Qu, D. Li, F.F. Tao, Z. Sun, ACS Appl. Mater. Interfaces 9 (2017) 18549–18556.
[17] X. Jia, J. Li, E. Wang, Nanoscale 4 (2012) 5572–5575.
[18] X. Wen, P. Yu, Y.R. Toh, X. Ma, J. Tang, Chem. Commun. 50 (2014) 4703–4706.
[19] K. Jiang, S. Sun, L. Zhang, Y. Lu, A. Wu, C. Cai, H. Lin, Angew. Chem. Int. Ed. 54 (2015) 5360–5363.
[20] S. Guan, R. Liang, C. Li, M. Wei, Talanta 165 (2017) 297–303.
[21] W. Cai, H. Gao, C. Chu, X. Wang, J. Wang, P. Zhang, G. Lin, W. Li, G. Liu, X. Chen, ACS Appl. Mater. Interfaces 9 (2017) 2040–2051.
[22] J. Ge, Q. Jia, W. Liu, M. Lan, B. Zhou, L. Guo, H. Zhou, H. Zhang, Y. Wang, Y. Gu, X. Meng, P. Wang, Adv. Healthc. Mater. 5 (2016) 665–675.
[23] W. Wang, L. Wang, Y. Li, S. Liu, Z. Xie, X. Jing, Adv. Mater. 28 (2016) 9320–9325.
[24] H. Chen, M. Song, J. Tang, G. Hu, S. Xu, Z. Guo, N. Li, J. Cui, X. Zhang, X. Chen, L. Wang, ACS Nano 10 (2016) 1355–1362.
[25] F. He, G. Yang, P. Yang, Y. Yu, R. Lv, C. Li, Y. Dai, S. Gai, J. Lin, Adv. Funct. Mater. 25 (2015) 3966–3976.
[26] C. Li, R. Liang, R. Tian, S. Guan, D. Yan, J. Luo, M. Wei, D.G. Evans, X. Duan, RSC Adv. 6 (2016) 16608–16614.
[27] W. Shang, C. Zeng, Y. Du, H. Hui, X. Liang, C. Chi, K. Wang, Z. Wang, J. Tian, Adv. Mater. 29 (2016) 1604381–1604289..
[28] H. Liu, Y. Xie, Y. Zhang, Y. Cai, B. Li, H. Mao, Y. Liu, J. Lu, L. Zhang, R. Yu, Biomaterials 121 (2017) 130–143.
[29] J. Wang, H. Zhao, Z. Zhou, P. Zhou, Y. Yan, M. Wang, H. Yang, Y. Zhang, S. Yang, ACS Appl. Mater. Interfaces 8 (2016) 19872–19882.
[30] Y. Chen, Y. Wu, B. Sun, S. Liu, H. Liu, Small 13 (2017) 1603446–1603460..
[31] H. Li, K. Fierens, Z. Zhang, N. Vanparijs, M.J. Schuijs, K. Van Steendam, N. Feiner Gracia, R. De Rycke, T. De Beer, A. De Beuckelaer, S. De Koker, D. Deforce, L. Albertazzi, J. Grooten, B.N. Lambrecht, B.G. De Geest, ACS Appl. Mater. Interfaces 8 (2016) 1147–1155.
[32] D. Chimene, D.L. Alge, A.K. Gaharwar, Adv. Mater. 27 (2015) 7261–7284.
[33] W. Chen, J. Ouyang, H. Liu, M. Chen, K. Zeng, J. Sheng, Z. Liu, Y. Han, L. Wang, J. Li, L. Deng, Y. –N. Liu, S. Guo, Adv. Mater. 29 (2017) 1603864–1603871.
[34] H. Fan, G. Yan, Z. Zhao, X. Hu, W. Zhang, H. Liu, X. Fu, T. Fu, X.B. Zhang, W. Tan, Angew. Chem. Int. Ed. 55 (2016) 5477–5482.
[35] T. Yin, J. Liu, Z. Zhao, Y. Zhao, L. Dong, M. Yang, J. Zhou, M. Huo, Adv. Funct. Mater. 27 (2017) 1604620–1604632.
[36] Q. Wang, D. O'Hare, Chem. Rev. 2012, 112, 4124–4155;
[37] W. Chen, B. Zhang, T. Mahony, W. Gu, B. Rolfe, Z.P. Xu, Small 12 (2016) 1627–1639.
[38] J. Sun, Y. Lei, Z. Dai, X. Liu, T. Huang, J. Wu, Z.P. Xu, X. Sun, ACS Appl. Mater. Interfaces 9 (2017) 7990–7999.
[39] S. Guan, Y. Weng, M. Li, R. Liang, C. Sun, X. Qu, S. Zhou, Nanoscale 9 (2017) 10367–10374.
[40] S. Guan, R. Liang, C. Li, D. Yan, M. Wei, D.G. Evans, X. Duan, J. Mater. Chem. B 4 (2016) 1331–1336.
[41] Z. Gu, J. J. Atherton, Z. Xu. Chem. Commun. 2015, 51, 3024–3036.
[42] R. Ma, Z. Liu, K. Takada, N. Iyi, Y. Bando, T. Sasaki, J. Am. Chem. Soc. 129 (2007) 5257–5263.
[43] Y. Wang, Y. Zhang, Z. Liu, C. Xie, S. Feng, D. Liu, M. Shao, S. Wang, Angew. Chem. Int. Ed. 56 (2017) 1–6.
[44] R. Tian, D. Yan, C. Li, S. Xu, R. Liang, L. Guo, M. Wei, D.G. Evans, X. Duan, Nanoscale 8 (2016) 9815–9821.
[45] X. Jia, Y. Zhao, G. Chen, L. Shang, R. Shi, X. Kang, G.I.N. Waterhouse, L. -Z. Wu, C.-H. Tung, T. Zhang, Adv. Energy Mater. 6 (2016) 1502585–1502591.

9

[46] X. Zheng, D. Xing, F. Zhou, B. Wu, W.R. Chen, Mol. Pharm. 8 (2011) 447–456.
[47] F. Li, T. Li, W. Cao, L. Wang, H. Xu, Biomaterials 133 (2017) 208–218.
[48] Y. Xu, Q. Liu, R. He, X. Miao, M. Ji, ACS Appl. Mater. Interfaces 9 (2017) 19653–19661.
[49] S. Valetti, J. Wankar, M.B. Ericson, A. Feiler, I. Manet, J. Mater. Chem. B 5 (2017) 3201–3211.
[50] J. Yu, B.R. Martin, A. Clearfield, Z. Luo, L. Sun, Nanoscale 7 (2015) 9448–9451.
[51] M. Hu, Y. Ju, K. Liang, T. Suma, J. Cui, F. Caruso, Adv. Funct. Mater. 26 (2016) 5827–5834.
[52] D. Yang, S. Song, Y. Zou, X. Wang, S. Yu, T. Wen, H. Wang, T. Hayat, A. Alsaedi, X. Wang, Chem. Eng. J. 323 (2017) 143–152.
[53] Y. Yang, X. Zhao, Y. Zhu, F. Zhang, Chem. Mater. 24 (2012) 81–87.
[54] H. Ding, S.B. Yu, J.S. Wei, H.M. Xiong, ACS Nano 10 (2016) 484–491.
[55] F. Würthner, T.E. Kaiser, C.R. Saha–Möller, Angew. Chem. Int. Ed. 50 (2011) 3376–3410.
[56] X. Song, H. Gong, T. Liu, L. Cheng, C. Wang, X. Sun, C. Liang, Z. Liu, Small 10 (2014) 4362–4370.
[57] Y. Wang, K. Wang, Z. Han, Z. Yin, C. Zhou, F. Du, S. Zhou, P. Chen, Z. Xie, J. Mater. Chem. C 5 (2017) 9629–9637.
[58] Y. Yang, J. Aw, B. Xing, Nanoscale 9 (2017) 3698–3718.
[59] J. Chen, J.S. Wei, P. Zhang, X.Q. Niu, W. Zhao, Z.Y. Zhu, H. Ding, H.M. Xiong, ACS Appl. Mater. Interfaces 9 (2017) 18429–18433.
[60] J. Ge, M. Lan, B. Zhou, W. Liu, L. Guo, H. Wang, Q. Jia, G. Niu, X. Huang, H. Zhou, X. Meng, P. Wang, C.S. Lee, W. Zhang, X. Han, Nat. Commun. 5 (2014) 4596–4603.
[61] L. Song, W. Shi, C. Lu, Anal. Chem. 88 (2016) 8188–8193.
[62] W. Liu, S. Xu, Z. Li, R. Liang, M. Wei, D.G. Evans, X. Duan, Chem. Mater. 28 (2016) 5426–5431.
[63] M. Zheng, Y. Li, S. Liu, W. Wang, Z. Xie, X. Jing, ACS Appl. Mater. Interfaces 8 (2016) 23533–23541.

Highlights

1: CDs/ICG-uLDHs agent exhibits combined multiple-modal imaging and high-efficiency therapy both *in vivo* and *in vitro* study.

2: The unique structure of uLDHs enabled to stabilize the photothermal agent and enhance its photothermal efficiency, while extending the fluorescence lifetime of carbon dots.

3: This work provides a simple and effective method in the design and fabrication of 2D ultrathin material with significantly enhanced biocompatibility fluorescent imaging properties and outstanding anticancer activity, which can be potentially applied in biomedical fields.

Graphical Abstract
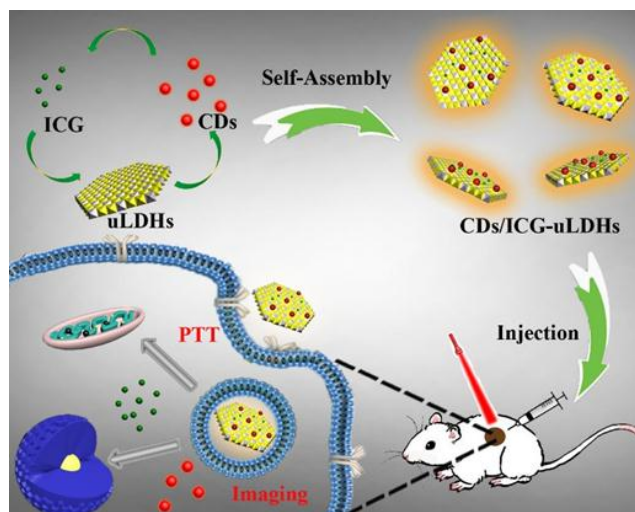
A multifunctional nanovehicle is synthesized by the self-assembly of carbon dots (CDs), indocyanine green (ICG) and ultrathin layered double hydroxides (uLDHs), which can be potentially used in triple-modal imaging and photothermal therapy.